Statistical Analysis of the Uncertainties in Cloud Optical Depth Retrievals Caused by Three-Dimensional Radiative Effects

TAMÁS VÁRNAI AND ALEXANDER MARSHAK

Joint Center for Earth Systems Technology of NASA Goddard Space Flight Center and University of Maryland Baltimore County, Greenbelt, Maryland

(Manuscript received 30 May 2000, in final form 20 October 2000)

ABSTRACT

This paper presents a simple yet general approach to estimate the uncertainties that arise in satellite retrievals of cloud optical depth when the retrievals use one-dimensional radiative transfer theory for heterogeneous clouds that have variations in all three dimensions. For the first time, preliminary error bounds are set to estimate the uncertainty of cloud optical depth retrievals. These estimates can help us better understand the nature of uncertainties that three-dimensional effects can introduce into retrievals of this important product of the Moderate Resolution Imaging Spectroradiometer instrument. The probability distribution of resulting retrieval errors is examined through theoretical simulations of shortwave cloud reflection for a set of cloud fields that represent the variability of stratocumulus clouds. The results are used to illustrate how retrieval uncertainties change with observable and known parameters, such as solar elevation or cloud brightness. Furthermore, the results indicate that a tendency observed in an earlier study—clouds appearing thicker for oblique sun—is indeed caused by three-dimensional radiative effects.

1. Introduction

Satellite measurements of the solar radiation reflected by clouds are often used to retrieve cloud properties such as the amount of liquid water in the clouds and the size of cloud droplets. Current retrieval algorithms are based on one-dimensional (1D) radiative transfer theory, which assumes that there is a one-to-one relationship between cloud reflective and physical properties. Common everyday experience, however, tells us that clouds often feature fully 3D structures with strong variabilities in both horizontal and vertical directions. Radiative interactions among nearby elements of heterogeneous clouds can upset the one-to-one relationships between cloud reflection and physical properties, so any measured brightness can be associated with a variety of cloud properties. Current retrievals avoid potential ambiguities by ignoring 3D effects and using the clear relationships of 1D radiative transfer instead—but as numerous theoretical studies (e.g., Davies 1984; Kobayashi 1993; Barker and Liu 1995) and several observational results (e.g., Loeb and Davies 1996; Loeb and Coakley 1998) indicate, this can introduce significant errors into the retrievals. A different approach to resolving retrieval ambiguities is to determine not a single best-guess value, but rather, the statistical parameters of the distribution of possible values. This approach has been used recently to estimate leaf area index and the photosynthetically active radiation from space (Knyazikhin et al. 1998; Diner et al. 1999). The current paper examines this statistical approach for cloud optical thickness retrievals, focusing on the uncertainties that horizontal cloud variability introduces into retrievals based on 1D theory. This study thereby complements earlier studies that examined the influence of vertical cloud heterogeneities (e.g., Li et al. 1994; Platnick 2000).

Understanding the effects of using 1D radiative transfer theory is especially important, because recent improvements in measurement accuracy can lead to comparable improvements in retrieval accuracy only if the retrievals account for all relevant physical processes (Fig. 1). However, while the possibility that 3D effects can cause significant retrieval errors is widely accepted, the magnitude of these errors in various situations is yet to be determined. This paper presents a first attempt toward this goal: it describes a simple approach to assessing the influence of horizontal cloud variability on the operational processing (Nakajima and King 1990; King et al. 1997) of measurements by the Moderate Resolution Imaging Spectroradiometer (MODIS) instrument on board the TERRA satellite. In particular, the study examines the probability distribution of retrieval errors for stratocumulus cloud optical depth and describes a simple technique to set error bounds for the

Corresponding author address: Tamás Várnai, Code 913, NASA GSFC, Greenbelt, MD 20771.
E-mail: varnai@climate.gsfc.nasa.gov

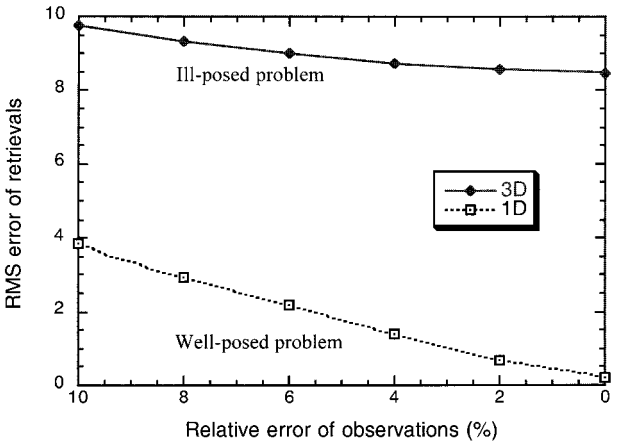

FIG. 1. Rms error of optical depth retrievals. The dashed line shows the errors when all the relevant physical processes are fully represented in retrievals based on 1D radiative transfer theory (1D real clouds). Note that the rms tends to zero as the observational accuracy increases, indicating that this situation is a ''well-posed'' problem. In contrast, the solid line corresponds to 3D real clouds, and the rms does not tend to zero even for perfectly accurate observations. This is an ''ill-posed'' problem (Twomey 1977). The figure is based on a sample set of radiative transfer calculations carried out at 250-m resolution for 60° solar zenith angle.

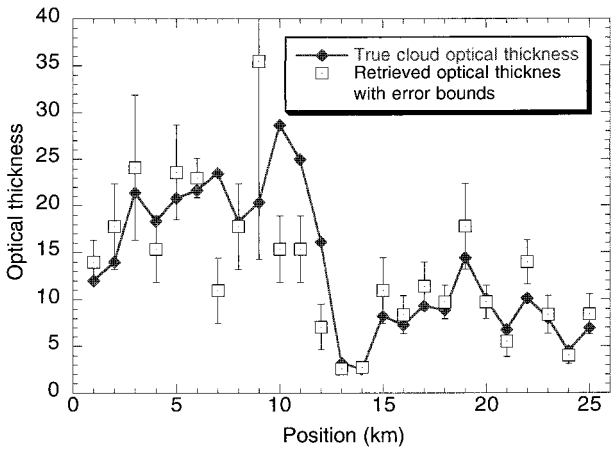

FIG. 2. Example for estimating the uncertainty of optical depth (τ) retrievals at 1-km resolution. The error bars indicate the estimated standard deviation of retrieval errors, which, assuming a Gaussian frequency distribution of retrieval errors, contain the true τ value with a 68% probability. (In Gaussian distributions, the confidence level corresponding to one standard deviation is around 68%.) The solar zenith angle is 60°, and the sun is on the left side.

MODIS retrievals. Figure 2 illustrates these error bounds and shows that while such error bounds cannot determine the retrieval errors for individual pixels (e.g., they do not show that the optical thickness is often overestimated on the sunlit slopes on the left side of cloud bumps and underestimated on the shadowy slopes on the right side), they can give statistically representative estimates on the magnitude of the errors.

The outline of this paper is as follows. First, section 2 describes the test dataset used in the proposed assessment algorithm. Then, section 3 outlines the algorithm's basic approach and also uses radiative transfer simulation results to highlight various features of the retrieval errors. Finally, section 4 summarizes the paper's main conclusions and outlines some possible directions for future work.

2. Test dataset

Since the proposed technique is based on a climatology of 3D effects that are obtained through radiative transfer simulations, it is very important to ensure that the simulations be representative of the processes that occur in the real atmosphere. The key issue is not whether 3D radiative processes can be calculated accurately, but whether the set of examined clouds is truly representative of the real clouds observed by satellites.

The biggest challenge in building a climatologically representative set of 3D cloud fields is that there are no suitable measurements of full 3D cloud structures. In situ aircraft measurements give only 1D transects, and passive measurements of the radiation leaving a cloud field cannot give detailed information on internal cloud structure. In addition, these passive measurements can be affected by the very same 3D effects we are trying to understand. Although in principle, active sensors (i.e., lidars and cloud radars) could determine 3D cloud structures, current systems give information only in the vertical and one horizontal direction, leaving cloud variability in the other horizontal direction unknown. Evans et al. (2000) presented a first attempt to overcome this limitation by developing a stochastic cloud model to extend the measured cloud fields to the unknown horizontal dimension.

The present study examines the statistical properties of 3D cloud fields that were generated by three different stochastic cloud models: the bounded cascades (Cahalan et al. 1994; Marshak et al. 1994, 1995), the fractionally integrated cascades (Schertzer and Lovejoy 1987), and filtering Gaussian noise in Fourier space with a power law (Evans 1993). (After the filtering, this third model transforms the field back to physical space and resamples it to obtain a scene with a Gamma or lognormal probability distribution function that has the desired parameters.)

The main common property of the above cloud models is scale invariance or scaling that has been systematically observed in real clouds (e.g., Cahalan and Snider 1989; Davis et al. 1994). The simple scaling means that the average change in cloud properties (such as optical depth τ) over distances Δx and $\lambda\Delta x$ (with λ being any positive number) can be related through (e.g., Vicsek 1989, p. 33)

$$\langle |\tau(x) - \tau(x + \lambda\Delta x)| \rangle \sim \lambda^H \langle |\tau(x) - \tau(x + \Delta x)| \rangle, \quad (1)$$

where the $\sim$ sign means statistical equality and $\langle\ \rangle$ indicates ensemble averaging over many realizations. For

stochastically continuous models H is required to be positive (e.g., Papoulis 1965, p. 312), and typical H values observed for the liquid water content of stratocumulus clouds vary between 0.25 and 0.4 (Marshak et al. 1997).

Broken cloud fields were simulated either by a cutting technique (Barker and Davies 1992; Marshak et al. 1998) or by the resampling technique where all values are transformed to obtain the desired histogram. We should note that the simulated broken cloud fields are no longer exactly scale invariant, and they follow the power-law scaling of Eq. (1) only approximately.

The models' input parameters are chosen such that they represent the observed average characteristics and variability of cloud properties. Because the main goal for this study was to generate a set of scenes that seeks to cover the natural variability of stratocumulus cloud properties, the clouds range from thin to thick, from almost homogeneous to very heterogeneous, and from overcast to partially cloudy. All results presented in this paper are based on simulations for at least 300 scenes that each cover $(51.2 \text{ km})^2$ areas at 50-m resolution (pixel size). Each scene was generated using a different random number sequence and a different set of cloud variability parameters. For optical thickness fields, these parameters are the mean, the standard deviation, the scaling parameter H, and the cloud fraction. These parameters were chosen for each scene according to a random uniform distribution that is based on the range of variability reported in Barker et al. (1996) (see Table 1).

Once the optical thickness was obtained by a stochastic cloud model, the complete cloud structure was determined by assuming a flat cloud base and vertically constant volume extinction coefficient, and by calculating the geometrical cloud thickness (Δz) of each pixel according to the empirical formula that Minnis et al. (1992) established for stratocumulus clouds:

$$\Delta z = 0.08\tau - 0.04.$$

In order to represent cases where the τ and Δz fields are not well correlated, in half of the overcast scenes the τ field was regenerated after having obtained the Δz field, using still the same parameters but a different random number sequence.

Backward Monte Carlo simulations then calculated the reflection of 10 randomly chosen pixels in each scene—and so the presented results are all based on simulations for at least 3000 pixels.

Once a comprehensive dataset of such scenes is put together, realistic statistics of 3D radiative effects can be calculated by weighting data points from each scene according to how often the scene's parameters can be observed in real clouds. (As a result, data from scenes resembling typical clouds will receive large weights, whereas data from scenes similar to rare clouds will carry much less weight in the statistical calculations.) For an easier illustration of the proposed technique, all data points in this paper are displayed with an equal weight and are accordingly given equal weight in the statistical calculations. Sensitivity studies (not shown) indicated that while applying realistic weighting schemes (e.g., assigning less weight to increasingly heterogeneous scenes) can change the mean and standard deviation of retrieval errors, it does not modify the qualitative features discussed in this paper. In the future, one can calculate climatologically representative statistics on retrieval errors for several specific locations [such as the Atmospheric Radiation Measurement (ARM) program site in central Oklahoma and in the western Pacific] by comparing the variability of simulated scenes to variabilities observed in cloud radar measurements.

TABLE 1. Ranges considered for various parameters of cloud optical thickness variability.

Parameter H	0.25–0.5
Probability of partial cloud coverage	0.5
Cloud fraction for broken cloud scenes	≥ 0.7
Scene-averaged optical thickness	5.0–20.0
υ = (Mean/St dev)^2 overcast scenes	2.0–25.0
broken cloud scenes	0.5–4.0
Shape of optical thickness histogram	Lognormal for overcast scenes, modified Gamma for broken cloud scenes

The presented simulations assume nonabsorbing cloud droplets with a C.1 phase function and do not consider the effects of cloud-free air and the underlying surface. The cloud fields are specified at a 50-m resolution, below which scale the fields are assumed to be homogeneous. The results of Marshak et al. (1998) show that this assumption does not significantly change the calculated cloud radiative properties. Most simulations presented in this paper, however, obtained cloud reflection for $(250 \text{ m})^2$ pixels, thereby matching the resolution of the MODIS instrument. Except when noted otherwise, all presented results are for 60° solar zenith angle and nadir view. The calculated reflectance values are affected by random Monte Carlo simulation errors less than 0.01, which could be viewed to be similar to various random uncertainties in the interpretation of satellite measurements. However, the paper does not specifically consider factors other than horizontal cloud heterogeneity that could affect the accuracy of optical thickness retrievals (e.g., calibration errors). Such factors are discussed in Pincus et al. (1995).

3. Estimation of retrieval uncertainties

a. Magnitude of retrieval errors

As mentioned in the introduction, the main goal of the presented technique is to estimate the influence of 3D radiative effects on MODIS optical depth retrievals and to set error bounds on the retrieval results accord-

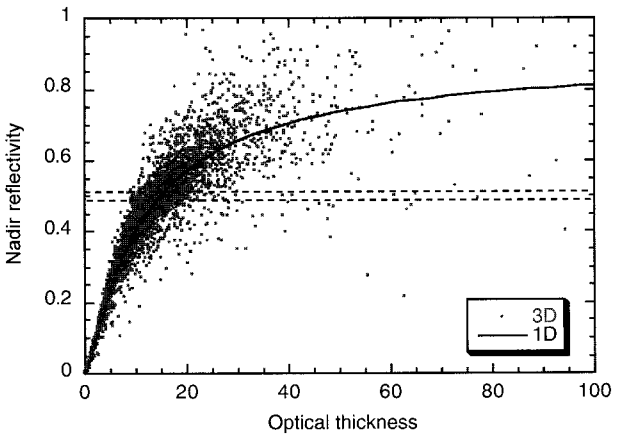

FIG. 3. Comparison of 1D and 3D nadir reflectivities over (250 m)^2 pixels for 60° solar zenith angle. The interval between the two dashed lines schematically illustrates the accuracy of observations.

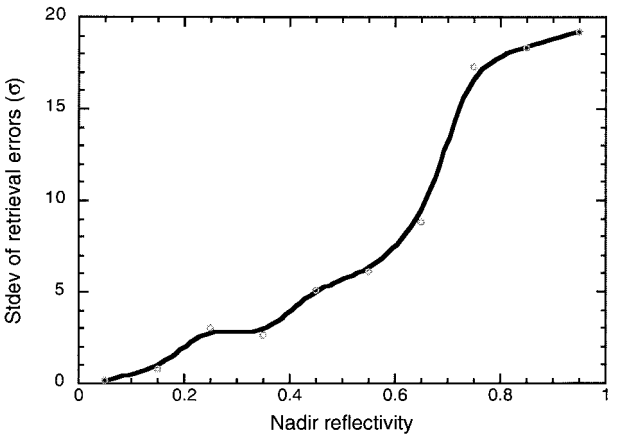

FIG. 4. Dependence of the standard deviation of retrieval errors (σ) of cloud optical thickness on cloud reflectivity. The bold curve shows a polynomial fit of the actual results.

ingly. The algorithm proposed to set the error bounds is illustrated in Fig. 3, which displays simulation results for a wide range of clouds. The operational MODIS algorithm works by determining which cloud optical thickness can yield the measured reflectivity value according to 1D radiative transfer theory, that is, according to the solid line in Fig. 3. The proposed assessment technique then estimates the retrieval uncertainty by considering a narrow brightness interval around the observed radiance (which represents the measurement accuracy and is indicated by horizontal dashed lines in the figure) and calculating how spread out the true optical thickness values yielding brightnesses inside the narrow interval are in the 3D simulations.

Figure 4 shows that generally, the standard deviation (σ) of the τ-retrieval errors (ε)—defined as

$$\sigma = \frac{1}{N-1}\sqrt{\sum_{i=1}^{N}(\varepsilon_i - \langle\varepsilon\rangle)^2}, \qquad (2)$$

with N being the number of pixels—increases with cloud reflectivity. This tendency is consistent with the findings of Pincus et al. (1995), who showed that retrieval errors caused by factors other than 3D effects increase with cloud brightness as well. The initial increase seems fairly intuitive, because the influence of 3D effects (which push the individual points away from the 1D curve) increases with the original 1D brightness it modifies. At larger brightnesses the increase accelerates because of the flattening of the 1D curve in Fig. 3: Since the brightness hardly changes with τ for thick areas, a given large brightness can occur for a wide range of τ values. This can be interpreted as a sign that at bright (i.e., thick) regions, the optical thickness and reflectivity (I) become decoupled from each other, and the brightness is determined not as much by τ, as by the local geometry that creates 3D effects (e.g., whether the examined slope tilts toward or away from the sun) (Várnai 2000). Finally, the spread of retrieval errors remains fairly constant at the brightest regions, because the 1D optical thickness retrievals are constrained by the arbitrary limit of not retrieving optical thicknesses greater than 100. Thus, further increases in cloud brightness do not lead to larger retrieval errors.

b. Magnitude and sign of retrieval errors

In addition to cloud brightness, retrieval uncertainties also depend on other factors, such as the sun-view geometry and the spatial resolution of reflectivity measurements. For example, Fig. 5 shows that, in agreement with the findings of earlier studies (e.g., Chambers et al. 1997; Davis et al. 1997; Zuidema and Evans 1998), the influence of 3D effects decreases with coarsening resolution, and at really coarse resolutions a 1D het-

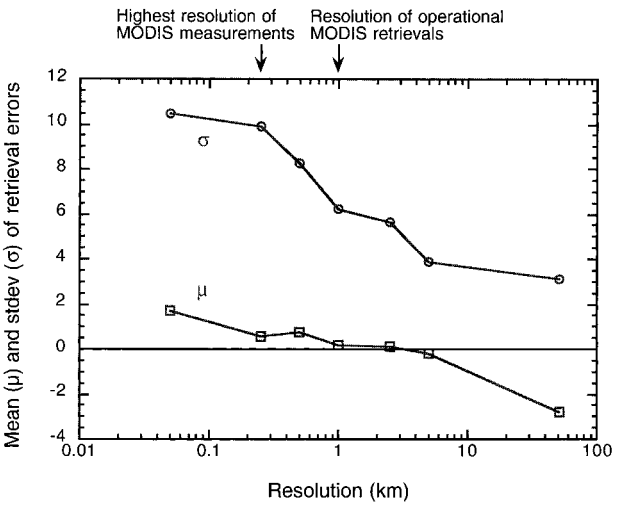

FIG. 5. Resolution dependence of retrieval errors. The mean error (μ) is defined simply as $\mu = 1/N\,\Sigma_{i=1}^{N}\,\varepsilon_i$, where the individual pixel retrieval error ε_i can be either positive or negative, and σ is defined by Eq. (2).

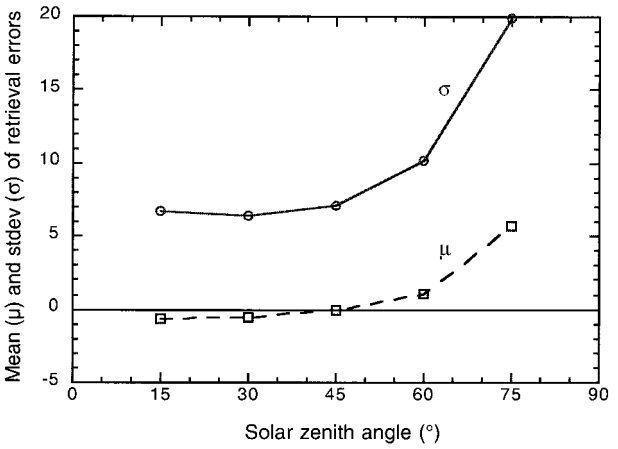

FIG. 6. Mean and standard deviation of retrieval errors for various solar zenith angles at 250-m resolution.

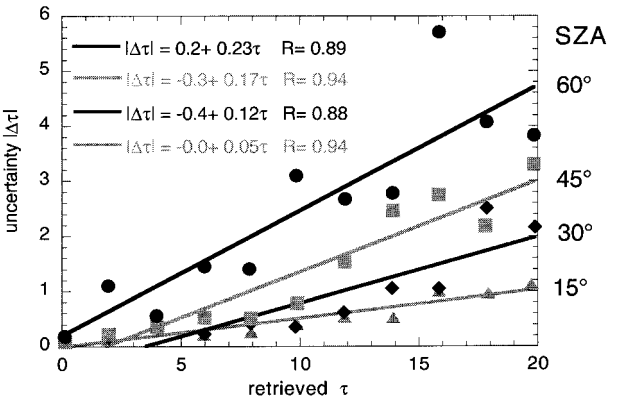

FIG. 7. The τ-dependence of retrieval uncertainties for various solar zenith angles.

erogeneity effect called the plane-parallel bias (Cahalan et al. 1994) becomes dominant. As a result, retrievals can be expected to be most accurate at intermediate resolutions in the order of a few hundred meters to a few kilometers (Davis et al. 1997). However, as Fig. 6 shows, retrieval errors due to 3D effects increase sharply for more oblique illuminations. This tendency causes the overestimations that are due to 3D effects to dominate over the underestimations that are due to the plane-parallel bias, even at resolutions as coarse as 30 km (Loeb and Davies 1996; Loeb et al. 1997; Varnai and Davies 1999).

In the range of optical thicknesses where the retrievals do not have an overall bias, the relative error of individual pixel retrievals is fairly steady for a given solar zenith angle (Fig. 7). This result suggests that in this range, the statistical expectation of the retrieval uncertainties ($\Delta\tau$) may be parameterized in a single linear form such as

$$\Delta\tau \approx \tau \times \frac{1}{3} \times \frac{\text{SZA}}{100^\circ}, \tag{3}$$

where SZA is the solar zenith angle.

The estimates mean that the correct value is inside the $\tau \pm \Delta\tau$ interval with 68% probability. For example, this formula estimates that for 30° solar zenith angle and $\tau = 20$, the uncertainty can be expected to be around 2. We should note, however, that this simple form may need adjustments for situations not considered in this study, such as different solar and viewing angles and spatial resolutions.

On the topic of systematic retrieval biases, Fig. 8 shows the relationship between the retrieved and the true mean optical thickness of all pixels that have a certain nadir reflectivity in 3D simulations

$$\tau_{\text{mean}}(I) = E(\tau|\,\text{reflectivity} = I), \tag{4}$$

where E is the mathematical expectation of the optical thickness retrieved using 1D theory [$\tau_{1D}(I)$]. The figure suggests that 1D retrievals give unbiased results for pixels that are not too bright. For brighter areas, however, using 1D theory results in an overestimation of the true mean optical thickness: when 3D effects enhance the brightness of thick slopes tilted toward the sun, 1D retrievals do not know about the tilting and must therefore assume very large optical thicknesses to account for the large brightness values. The fact that overestimations increase with cloud brightness is consistent with the observations of Loeb and Davies (1996), and further supports their assertion that the biases they observed are indeed caused by 3D radiative effects.

The fact that τ retrievals based on single reflectivity values cannot yield accurate results for thick or bright areas is also illustrated in Fig. 9. The figure shows that the

$$I_{\text{mean}}(\tau) = E(I_{3D}|\,\text{optical depth} = \tau) \tag{5}$$

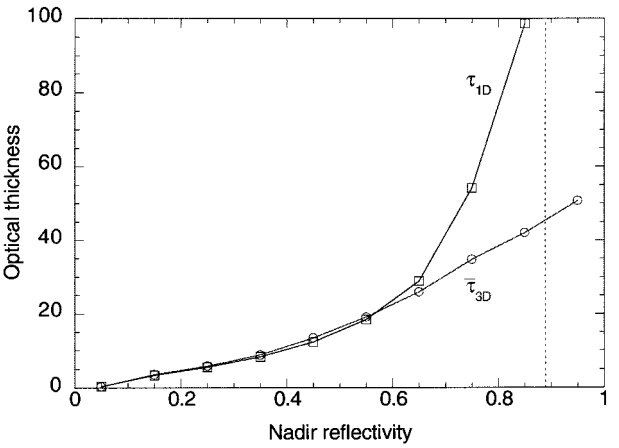

FIG. 8. Mean of true optical thickness in heterogeneous scenes (3D), and the value retrieved using one-dimensional theory (1D). The vertical dashed line represents the maximum nadir reflectance value that is possible in 1D radiative transfer. Note that this maximum nadir reflectance value (obtained for an infinitely thick cloud) is less than the maximum possible albedo of 1, because most of the reflected radiation goes in forward scattering directions, and relatively less goes toward the zenith.

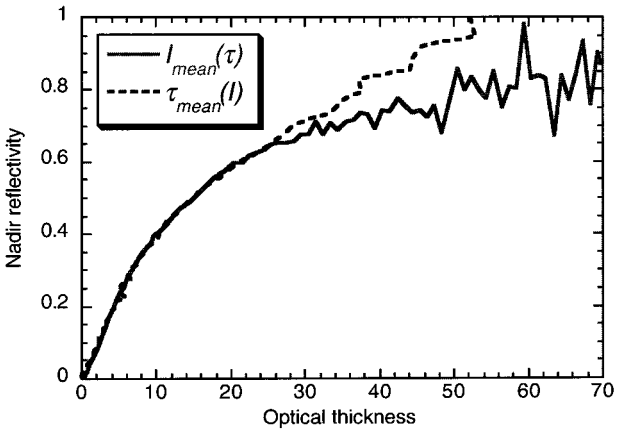

FIG. 9. Comparison of the $I_{mean}(\tau)$ and the $\tau_{mean}(I)$ curves obtained from averaging over all available pixels in 3D simulations for 60° solar zenith angle and 250-m resolution.

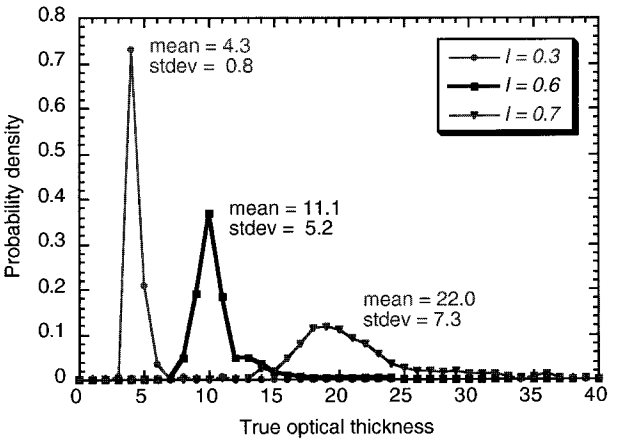

FIG. 10. Histogram of true optical thickness values for various reflectivity intervals.

and the $\tau_{mean}(I)$ curves diverge for $\tau > 25$ (i.e., $I > 0.65$), indicating that the mean τ–I relationship becomes nonreversible (Zhang et al. 2000).

In addition to considering the basic statistics of the true τ distribution as a function of cloud brightness, one can also examine the full τ histograms for fixed I values (Fig. 10). [Similar histograms of leaf area index values can be found in Knyazikhin et al. (1998).] The histograms clearly illustrate the tendency shown in Fig. 4: that the brighter a pixel is, the wider the histogram of possible τ_{true} values is, and so the harder it is to estimate the pixel's true optical depth. Figure 10 also shows that the histograms can be quite asymmetric, that is, underestimations and overestimations follow different probability distributions. This asymmetry is especially interesting for dark pixels ($I = 0.3$), where the histogram's tail on the left side is almost completely missing. (This tail contains pixels that are extra bright because they are on a sunlit slope.) Naturally, any tail on the left is limited by the fact that τ cannot go below zero. However, Fig. 10 shows that the histogram does not reach this limit, which means that another factor must restrict the tail on the left side well above the zero value. The fact that the tail on the left is smaller for less bright pixels can be explained as follows. In bright (and generally, thick) areas, pixels can gain significant extra illumination if the pixel in front is thinner, since this allows more incoming radiation to reach their sides. In darker (and generally thinner) areas, however, having an even thinner pixel in front does not cause much brightening, because the pixel in front would allow plenty sunlight to reach the side of our pixel even if it was only as thin as our pixel, and not even thinner.

The main practical implication of the resulting skewness is that since the distribution of retrieval errors is asymmetric, optimal error bounds should be set differently for underestimations and overestimations. Such asymmetric error bounds were calculated following standard statistical techniques (e.g., Cowan 1998, p. 119). These empirical error bounds were set to ensure that the error for a randomly selected pixel lies inside the bounds with a 95% or 68% probability (which we denote by α), and lies outside the bounds on either side with a probability of $(1 - \alpha)/2$ (=0.025 and 0.16 for $\alpha = 0.95$ and 0.68, respectively). In practice, the bounds for underestimation (B_u) and overestimations (B_o) were determined empirically from the equations

$$\int_{-\infty}^{B_u} P(\Delta\tau)\, d(\Delta\tau) = \frac{1 - \alpha}{2} \quad \text{and} \tag{6}$$

$$\int_{B_o}^{\infty} P(\Delta\tau)\, d(\Delta\tau) = \frac{1 - \alpha}{2}, \tag{7}$$

where P is the uncertainty probability density function.

Figure 11 shows the error bounds calculated empirically for underestimations and overestimations, as well as the bounds estimated using the Gaussian assumption. The figure indicates that often there are significant differences between the three error bounds. (The saturation

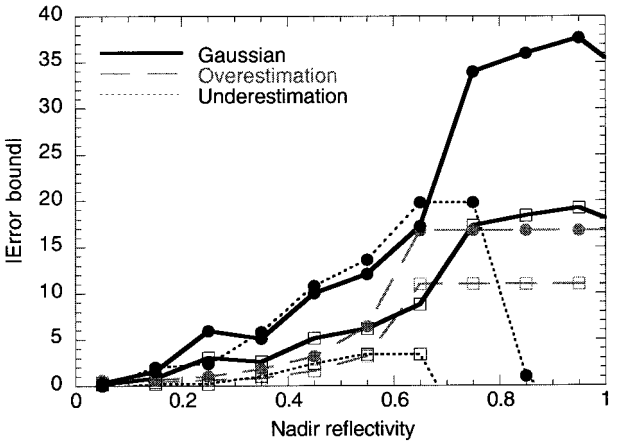

FIG. 11. Absolute values of error bounds for 95% ("=1.96 σ," full circles), and 68% ("=1 σ," empty squares) confidence levels.

of overestimation error bounds can be attributed to the fact that retrievals are limited optical thicknesses smaller than 100.) The figure also shows that the underestimation error bounds drop to zero at bright areas, which indicates that underestimations become very rare in these areas.

4. Conclusions

This paper presented results from a study that seeks to estimate the uncertainties that arise in satellite retrievals of cloud optical depth because retrievals are based on 1D radiative transfer theory and thus do not consider the effects of horizontal cloud variability. As a first step toward this goal, the paper examined the probability distribution of retrieval errors due to heterogeneity effects, as obtained from radiative transfer simulations over a wide variety of heterogeneous scenes. The examined scenes were generated by three different stochastic cloud models such that they represent the range of variability observed in stratocumulus clouds. Based on the simulated scenes, the rms error of optical thickness retrievals for (1 km)^2 pixels were estimated to be in the range of 3–5 for a solar zenith angle of 60°. The estimated error distributions were used to develop a simple technique that can set error bounds for operational cloud property retrievals. Figure 12 illustrates an example of error bounds estimated by applying the technique to MODIS Airborne Simulator (King et al. 1996) measurements.

The simulation results indicated that the retrieval uncertainties due to 3D radiative effects tend to increase with cloud brightness and solar zenith angle. For example, retrievals for 60° solar zenith angle gave unbiased overall averages for areas with nadir reflectivities less than 0.6, but the average optical thickness was increasingly overestimated for brighter regions. This behavior is consistent with the observations of Loeb and Davies (1996) and provides a further indication that the biases they observed were indeed caused by 3D radiative effects.

The results also suggested that when no overall bias affected the retrievals, simple linear parameterizations can give rough first estimates of the retrieval uncertainties.

Although the results showed that retrievals over relatively dark areas can be expected to be free of overall biases, the results also indicated that these areas can still be affected by another complication: that retrieval errors have skewed probability distributions. This finding is important when the uncertainty is characterized by error bounds for specific confidence levels, since it shows that optimal error-bounds should be set separately for underestimations and overestimations.

While the scenes used in the calculations cover a wide range of observed cloud field properties, they cannot be considered climatologically representative, since it is not known which scenes are important because they resemble real clouds that occur frequently, and which scenes are less important because they resemble very rare clouds. Thus, the next step in quantitatively estimating the uncertainties of satellite retrievals will be for us to assign weights to the simulated scenes by comparing their structure to radar measurements over the

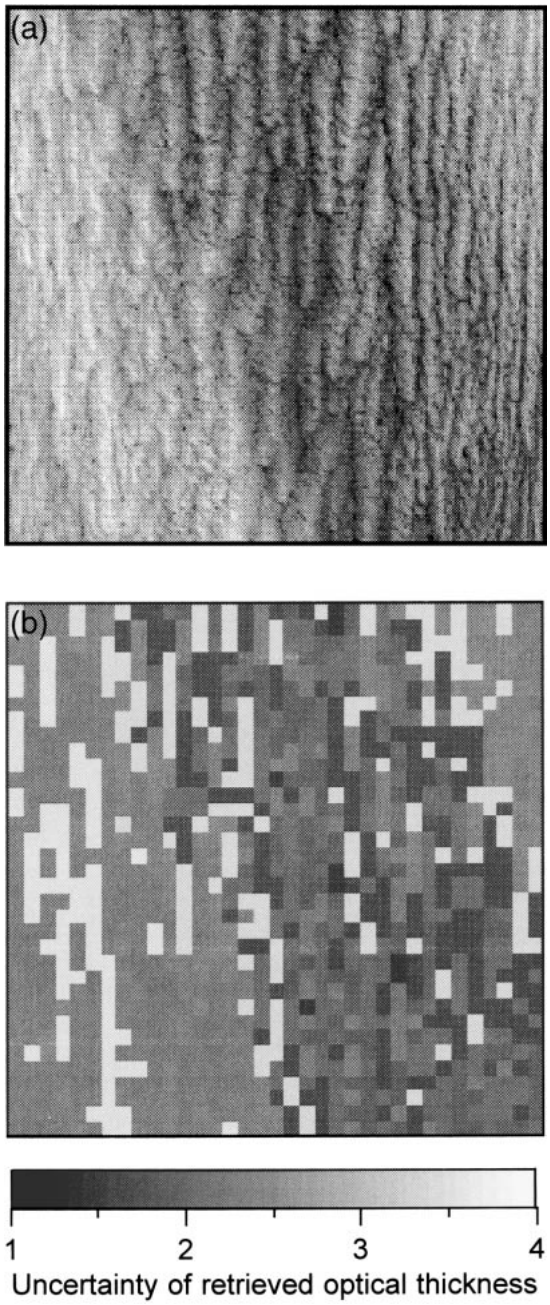

FIG. 12. Error estimates for a (35 km)^2 field of marine stratocumulus clouds: (a) original reflectivity field measured at 50-m resolution, and (b) estimated error bounds for optical thickness retrievals carried out at 1-km resolution. The error bonds were set to contain the actual retrieval errors with a 68% probability. Using 1D retrievals at 1 km resolution, the mean and the standard deviation of the optical thickness field are estimated to be 12.4 and 4.4, respectively.

ARM site in central Oklahoma and in the Western Pacific. This will enable us to refine the initial estimates of satellite retrieval uncertainty values that were presented in this paper.

Finally, the presented approach can be extended so that it estimates retrieval uncertainties by considering not only the brightness of each pixel, but also the spatial, angular, and spectral variability of cloud reflection. For this, one can examine how the additional information can enhance the reliability of error estimates for various sun-view geometries and cloud types. Our current efforts seek to determine whether the influence of 3D effects can be estimated using the phenomenon that 3D effects enhance local brightness variability more strongly at absorbing than at non-absorbing wavelengths (Oreopoulos et al. 2000). Promising preliminary results suggest that the reliability of estimated error bounds can be greatly improved by comparing the local variabilities measured at 0.86 μm and at the new MODIS wavelength at 2.13 μm. In addition, the early results also suggest that a simple test of local gradient values (i.e., whether a pixel is on a sunlit or shadowy slope) can predict whether the retrievals for specific pixels are affected by overestimation or underestimation.

Acknowledgments. We appreciate funding for this research from the NASA EOS Project Science Office at the Goddard Space Flight Center (under Grant NAG5-6675) and support from project scientist David O'C. Starr. We are also grateful to Yuri Knyazikhin, Anthony Davis, Steve Platnick, Frank Evans, and Robert Pincus for many fruitful discussions and to Laura Atwood for proofreading the manuscript and providing helpful suggestions.

REFERENCES

Barker, H. W., and F. A. Davies, 1992: Solar radiative fluxes for stochastic, scale-invariant broken cloud fields. *J. Atmos. Sci.*, **49,** 1115–1126.

——, and D. Liu, 1995: Inferring optical depth of broken clouds from Landsat data. *J. Climate,* **8,** 2620–2630.

——, B. A. Wielicki, and L. Parker, 1996: A parameterization for computing grid-averaged solar fluxes for inhomogeneous marine boundary layer clouds. Part II: Validation using satellite data. *J. Atmos. Sci.,* **53,** 2304–2316.

Cahalan, R. F., and J. B. Snider, 1989: Marine stratocumulus structure during FIRE. *Remote Sens. Environ.,* **28,** 95–107.

——, W. Ridgway, W. J. Wiscombe, T. L. Bell, and J. B. Snider, 1994: The albedo of fractal stratocumulus clouds. *J. Atmos. Sci.*, **51,** 2434–2455.

Chambers, L., B. Wielicki, and K. F. Evans, 1997: Accuracy of the independent pixel approximation for satellite estimates of oceanic boundary layer cloud optical depth. *J. Geophys. Res.,* **102,** 1779–1794.

Cowan, G., 1998: *Statistical Data Analysis.* Clarendon Press, 197 pp.

Davies, R., 1984: Reflected solar radiances from broken cloud scenes and the interpretation of satellite measurements. *J. Geophys. Res.,* **89,** 1259–1266.

Davis, A., A. Marshak, W. Wiscombe, and R. Cahalan, 1994: Multifractal characterizations of non-stationarity and intermittency in geophysical fields: Observed, retrieved, or simulated. *J. Geophys. Res.,* **99,** 8055–8072.

——, ——, R. Cahalan, and W. Wiscombe, 1997: The Landsat scale-break in stratocumulus as a three-dimensional radiative transfer effect, implications for cloud remote sensing. *J. Atmos. Sci.,* **54,** 241–260.

Diner, D. J., and Coauthors, 1999: New directions in Earth observing: Scientific applications of multiangle remote sensing. *Bull. Amer. Meteor. Soc.,* **80,** 2209–2228.

Evans, K. F., 1993: Two-dimensional radiative transfer in cloudy atmospheres: The spherical harmonics spatial grid method. *J. Atmos. Sci.,* **50,** 3111–3124.

——, S. McFarlane, and W. Wiscombe, 2000: A stochastic cloud field model for generalizing radar derived cloud structure for solar radiative transfer calculations. *10th Annual Atmospheric Radiation Measurement Program Science Team Meeting,* San Antonio, TX. [Available online at http:///www.arm.gov/docs/documents/technical/conf-0003/evans-kf.pdf.]

King, M. D., and Coauthors, 1996: Airborne scanning spectrometer for remote sensing of cloud, aerosol, water vapor and surface properties. *J. Atmos. Oceanic Technol.,* **13,** 777–794.

——, S.-C. Tsay, S. Platnick, M. Wang, and K.-N. Liou, 1997: Cloud retrieval algorithms for MODIS: Optical thickness, effective particle radius, and thermodynamic phase. MODIS Algorithm Theoretical Basis Document ATBD-MOD-05, Version 5, NASA, 83 pp.

Knyazikhin, Y., J. V. Martonchik, D. J. Diner, R. B. Myneni, M. Verstraete, B. Pinty, and N. Gobron, 1998: Estimation of vegetation canopy leaf area index and fraction of absorbed photosynthetically active radiation from atmosphere-corrected MISR data. *J. Geophys. Res.,* **103,** 32 239–32 256.

Kobayashi, T., 1993: Effects due to cloud geometry on biases in the albedo derived from radiance measurements. *J. Climate,* **6,** 120–128.

Li, J., D. J. Geldart, and P. Chylek, 1994: Solar radiative transfer in clouds with vertical internal inhomogeneity. *J. Atmos. Sci.,* **51,** 2542–2552.

Loeb, N. G., and R. Davies, 1996: Observational evidence of plane parallel model biases: Apparent dependence of cloud optical depth on solar zenith angle. *J. Geophys. Res.,* **101,** 1621–1634.

——, and J. A. Coakley, 1998: Inference of marine stratus cloud optical depths from satellite measurements: Does 1D theory apply? *J. Climate,* **11,** 215–233.

——, T. Várnai, and R. Davies, 1997: Effect of cloud inhomogeneities on the solar zenith angle dependence of nadir reflectance. *J. Geophy. Res.,* **102,** 9387–9395.

Marshak, A., A. Davis, R. F. Cahalan, and W. J. Wiscombe, 1994: Bounded cascade models as non-stationary multifractals. *Phys. Rev. E,* **49,** 55–69.

——, ——, ——, W. Wiscombe, and G. Titov, 1995: The verisimilitude of the independent pixel approximation used in cloud remote sensing. *Remote Sens. Environ.,* **52,** 72–78.

——, ——, ——, and R. Cahalan, 1997: Scale-invariance of liquid water distributions in marine stratocumulus. Part II: Multifractal properties and intermittency issues. *J. Atmos. Sci.,* **54,** 1423–1444.

——, ——, ——, and ——,1998: Radiative effects of sub-mean free path liquid water variability observed in stratiform clouds. *J. Geophys. Res.,* **103,** 19 557–19 567.

Minnis, P., P. W. Heck, D. F. Young, C. W. Fairall, and B. J. Snider, 1992: Stratocumulus cloud properties derived from simultaneous satellite and island-based instrumentation during FIRE. *J. Appl. Meteor.,* **31,** 317–339.

Nakajima, T. Y., and M. D. King, 1990: Determination of the optical thickness and effective particle radius of clouds from reflected solar radiation measurements. Part I: Theory. *J. Atmos. Sci.,* **47,** 1878–1893.

Oreopoulos, L., A. Marshak, R. F. Cahalan, and G. Wen, 2000: Cloud 3D effects evidenced in Landsat spatial power spectra and autocorrelation functions. *J. Geophys. Res.,* **105,** 14 777–14 788.

Papoulis, A., 1965: *Probability, Random Variables and Stochastic Processes.* McGraw-Hill, 583 pp.

Pincus, R., M. Szczodrak, J. Gu, and P. Austin, 1995: Uncertainty in cloud optical depth estimates made from satellite radiance measurements. *J. Climate,* **8,** 1453–1462.

Platnick, S., 2000: Vertical photon transport in cloud remote sensing problems. *J. Geophys. Res.,* **105,** 22 919–22 935.

Schertzer, D., and S. Lovejoy, 1987: Physical modeling and analysis of rain and clouds by anisotropic scaling multiplicative processes. *J. Geophys. Res.,* **92,** 9693–9714.

Twomey, S., 1977: *Introduction to the Mathematics of Inversion in Remote Sensing and Indirect Measurements.* Elsevier Publishing Co., 243 pp.

Várnai, T., 2000: Influence of three-dimensional radiative effects on the spatial distribution of shortwave cloud reflection. *J. Atmos. Sci.,* **57,** 216–229.

——, and R. Davies, 1999: Effects of cloud heterogeneities on shortwave radiation: Comparison of cloud-top variability and internal heterogeneity. *J. Atmos. Sci.,* **56,** 4206–4223.

Vicsek, T., 1989: *Fractal Growth Phenomena.* World Scientific Publishing Co., 97 pp.

Zhang, Y., and Coauthors, 2000: Prototyping of MISR LAI and FPAR algorithms with POLDER data over Africa. *IEEE Trans. Geosci. Remote Sens.,* **38,** 2402–2418.

Zuidema, P., and K. F. Evans, 1998: On the validity of the independent pixel approximation for the boundary layer clouds observed during ASTEX. *J. Geophys. Res.,* **103,** 6059–6074.